A Tone-Mapping Technique Based on Histogram Using a Sensitivity Model of the Human Visual System

Ishtiaq Rasool Khan, Susanto Rahardja, *Fellow, IEEE*, Muhammad Murtaza Khan, *Member, IEEE*, Muhammad Mobeen Movania, and Fidaa Abed

***Abstract*—High-dynamic-range (HDR) images require tone mapping to be displayed properly on lower dynamic range devices. In this paper, a tone-mapping algorithm that uses histogram of luminance to construct a lookup table (LUT) for tone mapping is presented. Characteristics of the human visual system (HVS) are used to give more importance to visually distinguishable intensities while constructing the histogram bins. The method begins with constructing a histogram of the luminance channel, using bins that are perceived to be uniformly spaced by the HVS. Next, a refinement step is used, which removes the pixels from the bins that are indistinguishable by the HVS. Finally, the available display levels are distributed among the bins proportionate to the pixels counts thus giving due consideration to the visual contribution of each bin in the image. Quality assessment using both quantitative evaluations and user studies suggests that the presented algorithm produces tone-mapped images that are visually pleasant and preserve details of the original image better than the existing methods. Finally, implementation details of the algorithm on GPU for parallel processing are presented, which could achieve a significant gain in speed over CPU-based implementation.**

***Index Terms*—High dynamic range (HDR), human visual system (HVS), image enhancement, tone mapping.**

I. Introduction

THE dynamic range (ratio of the maximum and the minimum luminance) of a real scene is often large and cannot be replicated correctly on most of the currently available displays. Though high-dynamic-range (HDR) displays are making their way in the market and their market share is increasing faster than ever, they are unlikely to replace all existing low dynamic range (LDR) displays in the near future. Over the past decade, a large number of tone-mapping operators (TMOs) have been introduced, which essentially function as intensities mapping of an HDR image to the target display range. In general, the LDR images produced through tone mapping contain more details of the scene than any single LDR shot taken at a fixed exposure [1]. Therefore, developing new algorithms for tone mapping has commercial potential and is still an active research area. Human visual system (HVS) models have been used for tone mapping and other image and video processing applications [2]–[21]. In this paper, a tone-mapping algorithm that uses an HVS sensitivity model is presented. The algorithm is computationally efficient and at the same time preserves both naturalness and structure of the original scene.

In general, TMOs can be classified into two major categories—global, which maps luminance solely based on its value, and local, which also takes local neighborhood features into account. Local tone-mapping algorithms, in general, are good at preserving the details by utilizing the local features in each region; however, they may induce halo and other artefacts [15]. Most of the studies such as Čadík *et al*. [22] and Cerdá-Company *et al*. [23] show a clear liking for the global tone mapping over the local algorithms by participating subjects. Global tone-mapping methods make use of a nondecreasing monotonic curve to map the HDR luminance to the display's range, thus making the transformation computationally efficient and artefact free. The algorithm presented in this paper is a global algorithm.[1]

Complementary to the passive tone mapping, some researchers have proposed interactive techniques that locate areas of interest based on cursor position or user's gaze. One earlier example was the work of Lischinski *et al*. [24], which allows the users to draw strokes on the image to see details of that region by adjusting the tonal values. Similarly, Farbman *et al*. [25] present a tool for interactive display of tone and contrast of details at different scales. In [26], a system that

Manuscript received April 11, 2017; revised July 7, 2017 and August 31, 2017; accepted September 11, 2017. Date of publication October 6, 2017; date of current version January 5, 2018. This work was supported by the Deanship of Scientific Research (DSR), King Abdulaziz University, Jeddah, under Grant 611-398-D1435. *(Corresponding author: Susanto Rahardja.)*

I. R. Khan is with the Faculty of Computing and IT, King Abdulaziz University, Jeddah, Saudi Arabia, and also with the Faculty of Computing and IT, University of Jeddah, Jeddah 21589, Saudi Arabia (e-mail: irkhan@kau.edu.sa).

S. Rahardja is with the Northwestern Polytechnical University, Xi'an 710072, China (e-mail: susantorahardja@ieee.org).

M. M. Khan and F. Abed are with the Faculty of Computing and IT, University of Jeddah, Jeddah 21959, Saudi Arabia (e-mail: mkhan@uj.edu.sa fabed@uj.edu.sa).

M. M. Movania is with the DHA Suffa University, Karachi 710072, Pakistan (e-mail: mobeen.movania@dsu.edu.pk).

Color versions of one or more of the figures in this paper are available online at http://ieeexplore.ieee.org.

Digital Object Identifier 10.1109/TIE.2017.2760247

[1]Code of the proposed algorithm can be downloaded from the website http://informatics-lab.com/att-algorithm/.

detects location of user's gaze and adjusts the tone-mapping operation accordingly was shown. In [27], a similar gaze-based technique for improving the tone-mapping performance is presented. Though the interactive techniques serve well for certain applications, they are not exactly suitable and well accepted yet for general purpose image displaying. More recent works on tone mapping [28] focus on HDR video; however, our focus in this study is on images only.

A popular global tone-mapping algorithm by Ferwerda *et al*. [16] proposes to use a visual adaptation model to fit the psychophysical results incorporating threshold visibility, color appearance, visual acuity, and sensitivity over time. Another method proposed by Drago *et al*. [17] is based on compression of luminance using a scene-dependent logarithmic basis to preserve contrast and details. One of the most commonly used global TMO is the work of Reinhard *et al*. [29], which focuses on giving pleasant photographic look to the results. Hateren [18] proposes a model of human cones for tone mapping of HDR videos and images. Reinhard and Devlin [19] construct a global operator based on photoreceptor response of the cones in the eye. A noteworthy algorithm presented by Kim and Kautz [30] is based on the assumption that human visual sensitivity follows Gaussian distribution and depends on average log luminance of the scene. Kim *et al*. [31] model the tone-mapping curves in two-dimensional (2-D) and three-dimensional (3-D) modes in piecewise linear form for RGB channels and normalizes them to reduce distortions in the color contrast in 3DTV. Lenzen *et al*. [32] present a preference model of human viewers to enhance the existing TMOs to produce visually pleasing results. Kim *et al*. [33] use weighted least square filters and neural networks to preserve pixel colors in the tone-mapped images.

Our tone-mapping algorithm presented in this paper has its foundation based on one of the promising and earliest works in this domain—a histogram-based global TMO by Larson *et al*. [34]. The preference of working on a "histogram adjustment" method arises from the fact that it is fully automatic and independent of user-defined parameters or image-based dependencies. However, familiar histogram equalization-related problems, particularly, extreme contrast enhancement of highly populated bins (luminance levels) and intensive compression of sparsely populated bins, affect the usability and quality of results obtained using histogram-based techniques. To address these issues, the human visual sensitivity, which is modeled as a function of visual adaptation is incorporated in construction of the histogram [35]. This means that instead of using equispaced bins in linear or log luminance space, the visual sensitivity model is utilized to form the bins of the histogram, which are equispaced in terms of *just noticeable differences* (JNDs). This leads to grouping of visually similar intensities and their mapping to nearly same LDR values and, hence, to reduction of visual artefacts. Furthermore, the bin-counts are refined by removing the pixels, which are visually indistinguishable from other pixels in the same bin. This gives due weight to the visual contribution of each bin in construction of the tone-mapping curve.

To validate the performance of the aforementioned TMO algorithm (hereinafter called "Adaptive TVI-TMO Algorithm" or "ATT Algorithm"), we compare it with some existing state of the art methods. The quantitative evaluations assign highest scores to the ATT, and the results are ratified by the qualitative user evaluation. An advantage of the ATT algorithm is that in its final form it simply uses linear interpolation and a lookup table (LUT) to map from higher to lower dynamic ranges, thereby making it computationally efficient and practical for use in handheld devices. The complexity is linear to the number of pixels which is the best (within a constant multiplying factor) that can be achieved for a tone-mapping algorithm. However, for large images, the execution time of sequential implementation on CPU can be slow. We present an implementation of the ATT algorithm on a GPU, which can perform processing in parallel and make the execution faster enough for real-time applications.

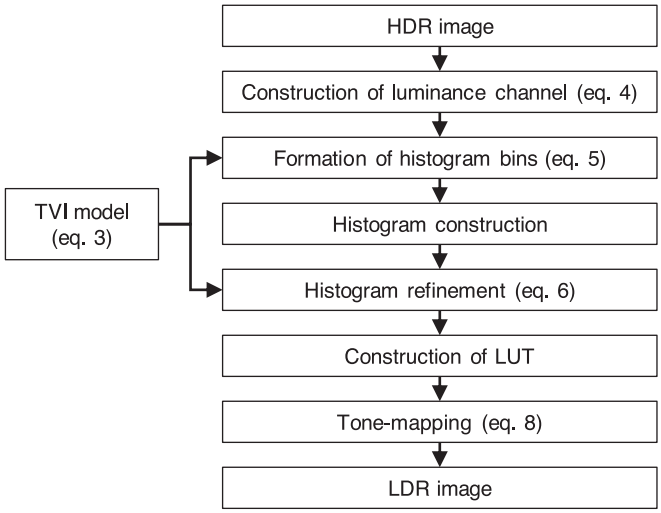

Fig. 1. Block diagram giving step-by-step description of the presented ATT algorithm.

The rest of the paper is organized as follows. Section II gives a brief description of the histogram adjustment technique and the eye sensitivity model and a detailed description of the adaptive TVI-TMO algorithm. Some experimental evaluations are presented in Section III. Implementation of the algorithm on parallel structures, especially the GPU, is detailed in Section IV. Conclusions are given in Section V.

II. Adaptive TVI-TMO Algorithm

Here, for completeness, the adaptive TVI-TMO algorithm is presented, which is computationally efficient and outperforms existing methods in terms of producing natural-looking images and preserving details. A block diagram showing step-by-step procedure of the ATT algorithm is shown in Fig. 1, and a detailed description of the main concepts and their rationale is presented later in this section.

A. Histogram Adjustment for Tone Mapping

A histogram-based technique was presented by Larson *et al*. [34] for mapping the intensities in an HDR scene to available LDR display levels, summarized as follows.

1) A histogram of image luminance in $\log_{10}$ domain is constructed.

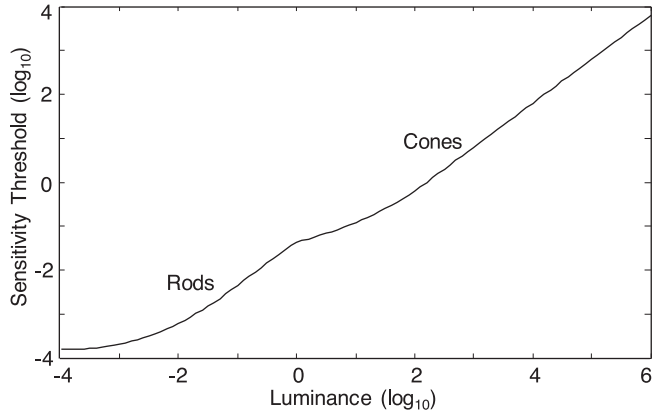

Fig. 2. TVI curve giving sensitivity of the HVS at different adaptation levels of luminance.

2) Denoting $f(b_i)$ as the pixel count in a bin b_i, a cumulative probability function is defined as

$$P(b) = \frac{1}{T}\sum_{b_i<b} f(b_i) \qquad T = \sum_{b_i} f(b_i). \quad (1)$$

3) A world luminance L_w of a pixel (x, y) in the HDR image is mapped to an LDR display luminance L_d in the range of $\min(L_d)$ to $\max(L_d)$ using the following equation:

$$L_d(x,y) = \min(L_d) + (\max(L_d) - \min(L_d))\, P(L_w(x,y)). \quad (2)$$

This assigns display levels to bins (groups of HDR luminance) based on their size (count of pixels). This is a very simple and intuitive method but has certain drawbacks, as will be mentioned later in this section, along with an approach to overcome them.

B. Visual System Adaptation and Sensitivity

The HVS is capable of viewing a huge range of luminance by adaptively adjusting to various conditions. A recent paper by Kim *et al*. [37] models the impact of ambient conditions on the perceived luminance and chrominance, and uses it to improve visibility of display of mobile devices in outdoor. Earlier models using similar psychophysical studies have been developed to determine JND perceived by human eye at a given adaptation level. The illumination change corresponding to a JND plotted versus the adaptation illumination on a log–log scale is known as threshold versus intensity (TVI) curve and is shown in Fig. 2.

Kundu and Pal [38] identify the following four different regions of the TVI curve: 1) very dark; 2) De Vries-Rose; 3) Weber; and 4) saturated. They approximate the TVI curve with a piecewise linear model. Later a nonlinear model was proposed by Ferwerda *et al*. [16] and further refined by Ward [39] as per DICOM standards spelled out in [40]. The resultant modified formulas for the TVI curve defining all the four regions are as follows:

$$\log_{10}(\delta L_a) = \begin{cases} -3.81, & \text{if } \log_{10}(L_a) < -3.94 \\ (0.405\log_{10}(L_a) + 1.6)^{2.18} - 3.81 & \\ \qquad \text{if } -3.94 \le \log_{10}(L_a) < -1.44 & \\ \log_{10}(L_a) - 1.345, & \\ \qquad \text{if } -1.44 \le \log_{10}(L_a) < -0.0184 & \\ (0.249\log_{10}(L_a) + 0.65)^{2.7} - 1.67 & \\ \qquad \text{if } -0.0184 \le \log_{10}(L_a) < 1.9 & \\ \log_{10}(L_a) - 2.205, & \text{if } \log_{10}(L_a) \ge 1.9. \end{cases} \quad (3)$$

In these equations, δL_a is the threshold value that would be perceived as a JND by the human eye adapted to a background luminance L_a. Both L_a and δL_a are in units of cd/m^2.

The TVI curve shown in Fig. 2 plots the sensitivity threshold of eye δL_a defined by (3) as functions of adaptation levels L_a in log–log domain. Note that if luminance is in scotopic or night vision range (-6 to -3 cd/m^2 in log domain), the rods in the eye play a more important role, whereas in photopic vision range (above 1 cd/m^2 in log domain), cones mechanism comes into play. In the intermediate mesopic vision conditions, both cones and rods work together. The model in (3) describes these characteristics of the HVS and has been shown to fit the experimental data very well [16], [39]. It can also be noted from Fig. 2 that some segments of the TVI curve at lower intensities are highly nonlinear, but for luminance levels above 1.9 cd/m^2 in log domain, the sensitivity threshold develops a linear relation with adaptation levels. However, the transition between different segments is not very abrupt. The model provides valuable insight of the functioning of the HVS sensitivity by providing accurate measure of JND at any adaptation level. This TVI model is used in the ATT algorithm to construct histogram, as explained next in detail.

C. JND-Based Histogram

In the histogram adjustment technique of [34], pixel clustering was done using equally spaced bins in log domain. However, as explained earlier with reference to [16], the visual sensitivity model in (3) suggests that this distribution of bins is not perceived to be uniform by the HVS. In view of this observation, this model is incorporated in constructing the image histogram by setting the bins to be equal to the number of JNDs wide. First, luminance of the input HDR image is calculated from its RGB channels as

$$\mathrm{HDR}_L = 0.265R + 0.670G + 0.065B. \quad (4)$$

Starting with the minimum value of HDR_L as the center of the first bin, new bins are formed such that the center of each new bin is equal number of JND steps away from the center of previous bin, until the maximum value of HDR_L is reached. The iterative process can be written as

$$b_{i+1} = b_i + n \cdot \delta b_i \quad (5)$$

where b_{i+1} is the center of the next bin which is n JND steps away from the center of the current bin. Width of a JND step

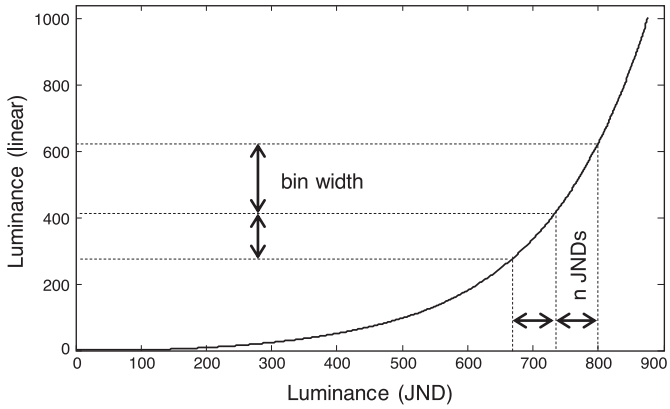

Fig. 3. Bin width in linear intensity domain plotted as function of JND. In bright regions, JND increases and bins get wider.

δb_i is determined by (3) by using the center of the current bin b_i as the adaptation level. Fig. 3 plots the values of bin centers b_i in linear domain which are equal number of JND steps apart. Note that a JND refers to different luminance change for each bin in the linear domain, and therefore the ATT bins are not uniformly distributed in linear domain, as can be observed from Fig. 3. However, they will be perceived to be approximately uniform by the HVS. By grouping perceptually similar pixels together, we can expect them to remain at similar intensity level in the tone-mapped image.

Larson *et al*. [34] note that the histogram adjustment algorithm is insensitive to the number of bins, as long as they can obtain adequate resolution. They used 100 bins. Note that if the number of bins is too large then there is a possibility of large number of adjacent bins staying nearly empty, which can lead to intensive compression of their intensities. We carried out extensive set of experiments to observe the effect of number of bins on performance of the ATT algorithm and found that the ATT algorithm provides good results with 70–90 bins for all the images we tested. By adjusting the bin-width, the number of bins that would span the whole intensity range can be controlled. The ATT algorithm selects the appropriate bin width automatically by adjusting n in (5) to keep the number of bins in the desired range.

D. Refinement of the Histogram Based on HSV

A drawback of the histogram-based tone mappings is that when there is a large peak in the histogram, the contrast is enhanced instead of being compressed. This might result in artificial artefacts in some parts of image, while leaving others exceedingly compressed. It is interesting to note that Larson *et al*. [34] use TVI model to clamp the bin counts that exceed a certain maximum. However, the clamping does not weigh the actual number of pixels in the bin (any number beyond a maximum will be clamped to the same value). Moreover, the maximum limit is the same for all bins that have intensities beyond 1.9 in the log domain. This simple approach might work in some cases; however, a more sophisticated approach is required to get good tone-mapped results for different types of HDR images. It can also be argued that bin population alone

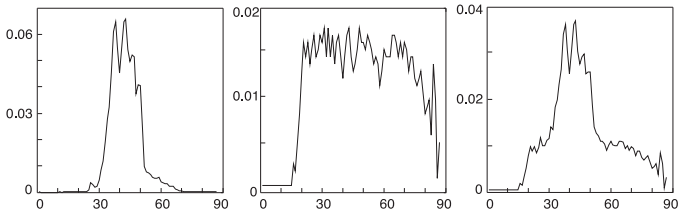

Fig. 4. From left to right, normalized bin counts in the actual histogram $f(b)$, refined histogram $r(b)$, and combined histogram $c(b)$ using $\omega = 0.4$, for a typical image with reference to (3).

is not always an optimal basis for allocation of display levels. Consider, for example, a large proportion of an image consisting of very similar pixels, say a pure white sky. It is not wise to allocate display levels to this region proportional to its size, without the visual contribution taken into account.

Instead of placing a ceiling on the bin's pixel count, the ATT bins are refined by counting all the pixels of extremely close intensities that are within a JND as one. This can be done in a single pass by arranging the pixels in ascending order of luminance, and removing those that are within a JND from the previous representative level. By doing so, the problems of contrast enhancement in densely populated bins and intensive compression in sparse bins are effectively resolved to a large extent. A new histogram is constructed by taking the weighted sum of the original and the refined histograms, given as

$$c(b) = \omega f(b) + (1-\omega) r(b) \tag{6}$$

where $f(b)$ and $r(b)$ are the pre- and the postrefinement counts, respectively, in bin b; ω and $(1-\omega)$ are the weights assigned to them, respectively; and ω can take a value in [0, 1] range. Note that both pre- and postrefinement counts are bounded in [0, 1] range; therefore, complimentary weights in [0, 1] range are assigned to them to keep the combined histogram bounded in the same range. Fig. 4 shows the histograms $f(b)$, $r(b)$, and $c(b)$ for a typical image, using $\omega = 0.4$. Note that some bins with very low counts originally get higher counts in the combined histogram $c(b)$, and therefore, details in the corresponding image segments would be better protected during tone mapping. However, it should also be noted that this comes at the cost of lowering the count in more populated bins, thereby reducing the number of display levels allocated to them, leaving them more prone to artefacts. In our experiments, a value of ω around 0.9 produced more natural results, whereas a lower value around 0.6 preserved the structure better. We found a good tradeoff is achieved at $\omega = 0.8$ for which the results are visually pleasing for almost all the test images and at the same time the structure is quite well preserved.

E. Implementation

A cumulative histogram assigns the cumulative number of counts in all the bins up to the current bin. We form a cumulative histogram $C(b)$ of the combined histogram $c(b)$ constructed in

(6), as follows:

$$C(b_i) = \begin{cases} 0, & i = 0 \\ \sum_{j=1}^{i} c(b_j), & 0 < i \leq N \end{cases} \tag{7}$$

where N is the number of bins in $c(b)$. Note that the cumulative histogram $C(b)$ has $N + 1$ bins.

For implementation of the tone-mapping algorithm, we construct an LUT with two columns and $N + 1$ rows. The first column contains the edges of the histogram bins (HDR values) and the second column contains the weights assigned to the cumulative histogram $C(b)$ in (7). We normalize them in a range 0 to the maximum LDR value (255 for 8 bit images). Two columns of the LUT now contain the pairs of HDR and the corresponding LDR values. Linear interpolation can be performed based on the pairs in this table to map each HDR value in the input image to LDR.

One way of tone mapping is to map the HDR luminance channel HDR_L obtained from (4) using the LUT to LDR luminance LDR_L and use the ratio of the two to map each of the *R*, *G*, and *B* channels as

$$\mathrm{LDR}_{R,G,B} = \left(\frac{\mathrm{HDR}_{R,G,B}}{\mathrm{HDR}_L}\right)^s \cdot \mathrm{LDR}_L \tag{8}$$

where s is the saturation factor and has a value less than 1. This approach ensures that each channel of a pixel is multiplied with the same factor. However, the first term on the right-hand side of (8) can become larger than 1, and therefore, the tone-mapped values can go beyond the maximum LDR value for the pixels, which have large LDR_L. Although a smaller value of s controls this divergence to some extent, some values still go beyond the allowed maximum and require clipping or smooth gradual convergence. A second approach is to tone map each channel separately using the obtained LUT, without calculating LDR_L. In this case, no values go out of bound, and therefore, convergence or clipping is not required. This approach is more advantageous for applications that require inverse tone mapping, as it is simpler and more accurate to do it directly on individual channels without involving the ratio channel. We tried both and found that the first approach that uses the ratio channel produces colors that are slightly more vibrant; however, the results of the second approach look more natural for some images. Quality indices on average are almost similar for both cases. We use the first approach with $s = 0.67$ for the results presented in this study.

III. Experimental Evaluations

In this section, we present a detailed comparison of our algorithm with three existing global methods—histogram adjustment by Larson *et al*. [34], the photographic operator by Reinhard *et al*. [29], and the method proposed by Kim and Kautz [30]. In a recent study by Cerdá-Company *et al*. [23], [30] is found to produce significantly better results than other evaluated methods, while [29] is ranked as the third best overall and the second best among the global algorithms. We used the codes of [34] and [29] provided by the authors themselves [1]. For Kim's method, we used the code from the HDR Toolkit by Francesco Banterle (https://github.com/banterle/HDR_Toolbox). For all the three methods, we did not change the default parameters used in these implementations. Note that the parameter tweaking for individual images can lead to slightly different results; however, a forte of our method is that it does not require such tweaking. Some comparisons are presented with a recently published local method [21], and again the implementation code provided by the authors is used.

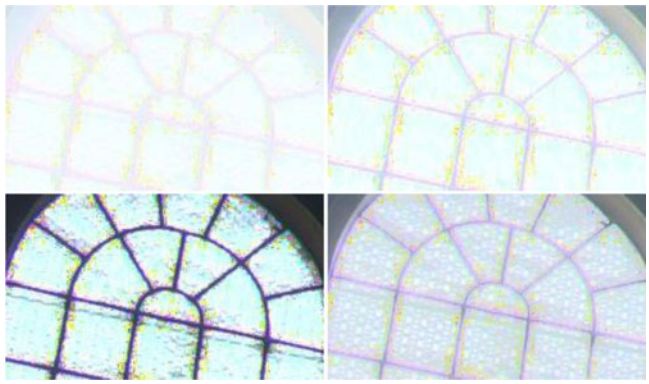

Fig. 5. Part of the HDR image *nancy_cathedral_1* tone mapped with the methods of Larson *et al.* [34], Reinhard *et al.* [29], Kim and Kautz [30], and the ATT algorithm (in the reading order).

A. Test Datasets

The HDR images dataset in the OpenEXR format on the accompanying disk of [1] comprises nine images, and we use it for both qualitative and quantitative analysis. This leads to the qualitative analysis with 63 image comparisons per subject, which is a reasonable-sized task. To further highlight the quality of results of the ATT algorithm, quantitative analysis on other larger datasets is also done. These datasets are 33 OpenEXR images of EMPA dataset [41], 42 RGBE images on the accompanying disk of [1], and 105 RGBE images of Funt *et al*. [42] dataset. Another dataset[2] was also used to obtain some results.

B. Visual Assessment

It can be understood from the earlier explanation that our algorithm suppresses the luminance in brighter regions and enhances it in darker regions. Thus, it tries to utilize the available display levels so that the representation mimics how a normal human eye would see the regions of the image after natural adaptation. Our experiments using different test datasets show that it can achieve a good balance between different regions and produce visually pleasing tone-mapped images compared to the other algorithms. Moreover, fine details of the scene are well preserved and colors are not saturated. Some results are shown in Figs. 5 and 6. In the window of the HDR image nancy_cathedral_1 shown in Fig. 5, details are best shown by the ATT algorithm. For the outdoor scene Oaks.hdr shown in Fig. 6, the ATT algorithm produces sharper image with clearer details—for example, observe the texture of trees and grass.

[2][Online]. Available: http://www.anyhere.com/gward/hdrenc/pages/originals.html

Fig. 6. Another HDR image *Oaks* tone mapped with the methods of Larson *et al.* [34], Reinhard *et al.* [29], Kim and Kautz [30], and the ATT algorithm (in the reading order).

C. Objective Assessment

Desirable characteristics of a TMO are that it should produce artefacts-free natural-looking results and preserve the structure. The tone-mapped image quality index (TMQI) [36] calculates the structural similarity and naturalness indices and then combines them to give an overall quality index. The naturalness index provides useful information regarding the correlations between image naturalness and different image attributes and can be computed as [36]

$$N = P_m P_d / K \tag{9}$$

where K is a normalization factor and P_m and P_d are the Gaussian and the Beta probability density functions, respectively, used to model the histograms of the means and standard deviations in the statistics conducted on a large database of 3000 natural images. For structural similarity, TMQI first calculates the local similarities between corresponding patches x and y of HDR and LDR image pairs as [36]

$$S_{\text{local}}(x,y) = \frac{2\sigma_x\sigma_y + C_1}{\sigma_x^2 + \sigma_y^2 + C_1} \cdot \frac{\sigma_{xy} + C_2}{\sigma_x\sigma_y + C_2} \tag{10}$$

where σ_x, σ_y, and σ_{xy} are the local standard deviations and the cross correlation between the corresponding HDR and LDR patches and C_1 and C_2 are the positive stabilizing constants. These similarities between patches are accumulated at different scales, and the obtained values at each scale are multiplied together to get an overall similarity measure S. The naturalness and structure similarity measures are combined to get an overall quality index as [36]

$$Q = a\, S^{\alpha} + (1-a)\, N^{\beta} \tag{11}$$

where $0 \le a \le 1$ adjusts the relative importance of the two components and α and β determine their respective sensitivities.

We compare our method with the three aforementioned algorithms using TMQI naturalness, structured similarity, and overall quality indices, in Tables I, II, and III, respectively. In each table, the winner algorithm's score is shown in bold font. In

TABLE I
TMQI SCORES FOR NATURALNESS OF THE TONE-MAPPED IMAGES

Image	Larson *et al.* [34]	Reinhard *et al.* [29]	Kim and Kautz [30]	ATT
BristolBridge	0.05209	0.07305	0.05417	**0.16456**
ClockBuilding	0.26317	0.56897	0.16638	**0.87809**
CrowFootGlacier	0.21036	0.19981	0.15534	**0.74557**
DomeBuilding	0.05735	0.24046	0.35084	**0.53422**
FribourgGate	0.18845	0.51025	0.42730	**0.78186**
MontrealStore	0.25010	0.39310	0.03625	**0.93723**
Moraine2	0.07614	0.13819	0.02671	**0.36215**
StreetLamp	0.10814	0.45546	**0**.64813	**0.89366**
Vernicular	0.08306	0.44350	0.47494	**0.76816**
Average	0.14321	0.33587	0.26001	**0.67394**

TABLE II
SCORES OF THE TMQI METRIC SHOWING STRUCTURED SIMILARITY OF THE TONE-MAPPED IMAGES WITH THE ORIGINAL IMAGES

Image	Larson *et al.* [34]	Reinhard *et al.* [29]	Kim and Kautz [30]	ATT
BristolBridge	0.77617	0.81827	**0.84473**	0.83238
ClockBuilding	0.82729	0.85095	0.85980	**0.86367**
CrowFootGlacier	0.85610	0.87262	**0.93949**	0.90296
DomeBuilding	0.68308	0.68776	0.73160	**0.86435**
FribourgGate	0.93694	0.93162	**0.94116**	0.93678
MontrealStore	0.90807	0.92826	**0.93227**	0.92038
Moraine2	0.87038	0.91140	**0.91782**	0.90688
StreetLamp	0.88302	0.87230	0.90252	**0.94128**
Vernicular	0.91050	0.91924	0.90659	**0.94250**
Average	0.85017	0.86582	0.88622	**0.90124**

TABLE III
TMQI OVERALL QUALITY SCORES OF THE TONE-MAPPING RESULTS

Image	Larson *et al.* [34]	Reinhard *et al.* [29]	Kim and Kautz [30]	ATT
BristolBridge	0.76617	0.78483	0.78623	**0.81298**
ClockBuilding	0.83341	0.89606	0.82093	**0.94752**
CrowFootGlacier	0.83001	0.83212	0.83922	**0.93812**
DomeBuilding	0.73959	0.78726	0.82307	**0.89388**
FribourgGate	0.84637	0.90749	0.89535	**0.95240**
MontrealStore	0.85245	0.88580	0.80320	**0.97108**
Moraine2	0.80007	0.82776	0.79579	**0.87447**
StreetLamp	0.81249	0.88239	0.92275	**0.97014**
Vernicular	0.81272	0.89263	0.89490	**0.95178**
Average	0.81036	0.85515	0.84238	**0.92360**

TABLE IV
AVERAGE TMQI QUALITY SCORES OF THE TONE-MAPPING RESULTS FOR OTHER DATASETS

Dataset	Larson *et al.* [34]	Reinhard *et al.* [29]	Kim and Kautz [30]	ATT
Reinhard (42 images)	0.8349	0.8810	0.8086	**0.9145**
EMPA (33 images)	0.7509	0.7800	0.7647	**0.8200**
Funt (105 images)	0.8023	0.8743	0.8485	**0.9172**

TABLE V
NUMBER OF TIMES EACH ALGORITHM STOOD THE BEST IN DIFFERENT DATASETS BASED ON TMQI QUALITY SCORES

Dataset	Larson [34]	Reinhard [29]	Kim [30]	ATT
Reinhard (42 images)	0	6	1	**35**
EMPA (33 images)	1	1	2	**29**
Funt (105 images)	0	11	8	**86**

terms of naturalness score (see Table I), the ATT algorithm produces best results for all images of the database. In terms of preserving structures of the original image (see Table II), all the four algorithms perform quite well. The algorithm of Kim and Kautz [30] and the ATT algorithm perform better for five and four images, respectively, but the average score of the ATT algorithm is the highest. In terms of overall quality (see Table III), the ATT algorithm again produces best scores for all the images. For these comparisons, we used the fixed default value of $\omega = 0.8$ in (6), although a slight variation for different images could further improve the results.

We also determined the quality of results of the ATT algorithm by using some other datasets. From Table IV, it can be observed that the overall TMQI value is the best for the ATT algorithm as compared to the other methods. Moreover, it can be seen from Table V that the ATT algorithm achieves best scores for a very large majority of images.

A relatively newer objective metric for tone-mapping quality assessment, FSITM [43], is based on comparison of the phase-derived feature maps of HDR and LDR images. Nafchi *et al.* [43] propose a combined TMQI–FSITM quality index that achieves better values of Spearman's rank-order correlation coefficient (SRCC) and the Kendall's rank-order correlation coefficient (KRCC) than TMQI and FSITM alone. We also compared the TMQI–FSITM quality indices of our method with other algorithms in Table VI for the OpenEXR dataset [1]. The results are similar to the TMQI-based evaluations given earlier. The ATT algorithm gets the best average score and wins for eight out of nine images.

All the methods compared earlier, including the ATT algorithm, perform global tone mapping. It would be interesting to see how the ATT algorithm fares against local methods, which are generally better in preserving structure of the scene but can produce artefacts. A retinex-based local TMO has been presented recently in [21] and shown to produce better TMQI scores compared to nine existing TMOs using another dataset.[2]

TABLE VI
TMQI–FSITM QUALITY SCORES OF THE TONE-MAPPING RESULTS

Image	Larson *et al.* [34]	Reinhard *et al.* [29]	Kim and Kautz [30]	ATT
BristolBridge	0.8191	0.8386	**0.8459**	0.8394
ClockBuilding	0.8369	0.8821	0.8545	**0.9034**
CrowFootGlacier	0.8552	0.8779	0.8816	**0.9125**
DomeBuilding	0.8043	0.8399	0.8548	**0.9032**
FribourgGate	0.8571	0.9063	0.9007	**0.9128**
MontrealStore	0.856	0.8861	0.8541	**0.9142**
Moraine2	0.8591	0.8893	0.8828	**0.9058**
StreetLamp	0.8569	0.8994	0.9198	**0.9412**
Vernicular	0.8605	0.9164	0.913	**0.9405**
Average	0.845	0.8818	0.8786	**0.9081**

TABLE VII
TMQI SCORES OF THE TONE-MAPPING RESULTS OF THE LOCAL TMO PUMA [21]

Algorithm	TMQI-Q	TMQI-S	TMQI-N
Puma (Color correction)	0.85486	0.80180	0.42578
Puma (No color correction)	0.87549	0.79884	0.54421
Puma Light (Color correction)	0.79136	0.76791	0.18647
Puma Light (No color correction)	0.81214	0.78901	0.22636
ATT	**0.92360**	**0.90124**	**0.67394**

The average quality indices reported in [21] for the two versions of their algorithm, Puma and Light Puma, are 0.8795 and 0.8871, respectively. We calculated the TMQI quality index score of the ATT algorithm for the same dataset, and it averaged to 0.9025, better than both the versions of the local TMO. We carried out further comparisons using the OpenEXR dataset used in our studies earlier, results of which are shown in Table VII. Although the local TMO produces some indices better than some of the algorithms compared in Tables I–III, the ATT algorithm still performs better than both versions of the local TMO for all three indices—naturalness, structure similarity, and overall quality.

D. Subjective Assessment

In order to qualitatively evaluate the performance of the ATT scheme, the ITUT Degradation Category Rating experiment using a group of 40 participants for the same OPENEXR dataset [1] as used in objective evaluations earlier is performed. The images were shown on a 32-inch LG monitor while the score keeping was done electronically, thus ensuring random sequence of image comparisons for each participant. The participants comprised of faculty and students from the computer science department but with no expertise in image processing. Two different experiments were conducted. In the first experiment, participants were asked to select between two images shown side by side based upon their preference. This resulted in obtaining a ranking of the tone-mapping methods that were compared. In a second experiment, all the four tone-mapping results were shown simultaneously to the participants and they were asked to rate each image on a scale from 0 (poor) to 10 (excellent).

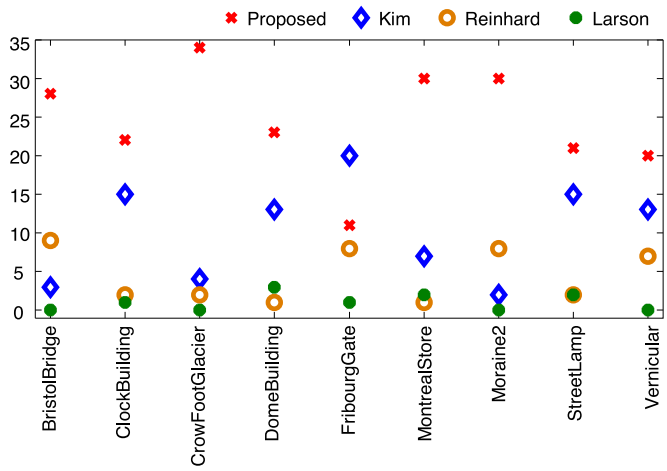

Fig. 7. Ranking of tone-mapping results by users for the test images. The *Y*-axis shows the number of users who rated the method as the best for a particular image.

The results of user preference by comparing two images at a time are presented in Fig. 7, which clearly shows that the users preferred the ATT algorithm result as the most, i.e., for eight out of nine images. These results are approximately in agreement with the TMQI results, where the results of the ATT algorithm are rated as the best in Table III. The users rated [30] as the second best followed by [29]. These results are approximately similar to the results shown in Table II where TMQI structure similarity rates [30] as second based on average scores and [29] as third.

Table VIII presents the median rating given by users to each image on a scale of 0.0 (poor) to 10.0 (excellent), when all the four images were shown simultaneously. The median values for the ATT algorithm are the best for all 9 images of Reinhard OpenEXR dataset. Here the users have rated Reinhard *et al.* [29] as the second best while Kim and Kautz [30] as third. This is in accordance with the naturalness and overall TMQI values presented in Tables I and III. Thus, both user studies corroborate the fact that the ATT algorithm has the best naturalness and overall visual quality as compared to other methods tested here.

IV. GPU Implementation

There are two major steps for performing the tone-mapping operation—design and application. This functional division also helps us in providing two basic parts of the GPU implementation namely *DesignTMO* and *ApplyTMO*. The *DesignTMO* function assumes that the HDR data are already loaded in the GPU texture memory. The steps involved in our GPU implementation of both functions are shown in Fig. 8. With these steps, the implementation of the ATT becomes very straightforward on a parallel architecture.

The steps 1, 2, 5, 7, 8, and 9 for the *DesignTMO* function can be implemented on the GPU using fragment shaders as they require point processing on a 2-D grid of pixels. All remaining steps (steps 3, 4, and 6) are better implemented on the CPU since they require divergent control flow which is slow on parallel architectures due to the CPU—GPU data transfer overhead. For the *ApplyTMO* function, step 1 requires interpolation of data using LUT, whereas step 2 performs point-by-point multiplication and division operations on 2-D arrays. Both steps can be implemented entirely in parallel using fragment shaders.

For all the steps using fragment shaders, the render to texture functionality is used. In the OpenGL API, this is exposed through the framebuffer object (FBO). Since the HDR data has high precision, render to floating point texture support is required which is now quite common on commodity graphics hardware. As is typically done in a GPGPU implementation, we first ensure that the model view and projection matrices are set up such that the render to texture functionality outputs to the entire output texture. We then bind the fragment shader, depending on the current step, pass all required input values (uniforms) and then render a full-screen quad of the size of the HDR input image. This executes the fragment shader on all input pixels in parallel, and we get the output stored in the GPU texture memory.

For calculation of the minimum and the maximum values, we use the parallel reduction approach as detailed in [44], which converges in $\log_2(n)$ steps, where n is the maximum of the number of rows and columns. The fundamental idea is to calculate minimum (or maximum) for the four neighboring pixels and then output the result on a texture ¼th the size of the original input texture. This is done until we have a 1×1 texture. The resulting value is then read back on the CPU to obtain the minimum (or maximum) value.

For generation of histogram on the GPU, we use the scattering-based approach detailed in [45] with additive blending (`glBlendFunc(GL_ONE, GL_ONE)`). We first enable render to texture support such that it outputs to a 1D texture of width equal to the total number of histogram bins. The texture for which the histogram is desired is input through render to vertex buffer (R2VB) technique to generate input attributes for the histogram vertex shader. The shader calculates the luminance value from the input color attribute and finds the appropriate bin. The fragment shader simply outputs a constant white color. With additive blending hardware, every time the output is written to a bin, the result is accumulated in the bin generating the histogram for the input texture.

Cumulative histogram is generated using a modification of the algorithm for generation of summed-area tables outlined in [46]. The fragment shader uses a simple sum shader that reads two pixels, the current pixel based on the assigned texture coordinates and another pixel "*stride*" pixels away. The *stride* is a shader uniform that is passed at each input iteration. Then, parallel reduction is carried out for k iterations where (`k = ceil(log2(N))`) for a histogram containing N bins. The process starts with a *stride* of 1. At each iteration, the *stride* is doubled. This way, we repeatedly sum two bins *stride* distance away until all histogram bins have been summed. For this to work, we have to ensure that the out of range texture accesses return 0 so that the output sum is correct. This is specially required for the boundary pixels of histogram. This can be ensured by setting the texture wrapping mode to clamp to border (`GL_CLAMP_TO_BORDER in OpenGL`) with a border color of (0,0,0,0).

TABLE VIII
MEDIAN SCORES BY PARTICIPANTS FOR THE TONE-MAPPED IMAGES

	BristolBridge	ClockBuilding	CrowFootGlacier	DomeBuilding	FribourgGate	MontrealStore	Moraine2	StreetLamp	Vernicular
ATT	**8.6**	**8.2**	**9.5**	**9**	**9.2**	**8.9**	**9.5**	**9.3**	**9.3**
Kim and Kautz [30]	6.6	7.1	6.9	6.2	7.2	7.1	5.7	7.1	7.0
Reinhard *et al*. [29]	7.0	7.5	7.5	7.7	7.2	7.8	7.5	7.5	7.0
Larson *et al*. [34]	3.6	3	3.5	3.3	3	4.0	5.2	3.0	2.9

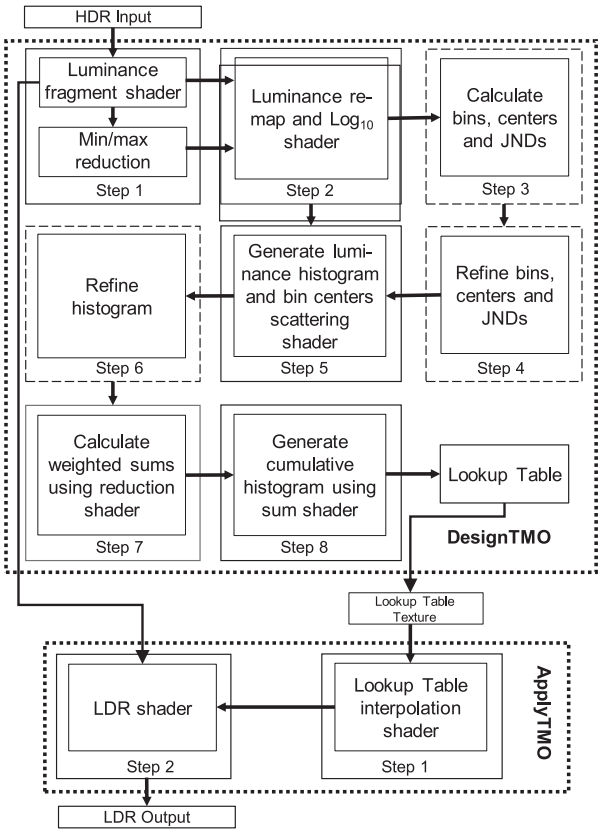

Fig. 8. GPU mapping of the ATT algorithm. The solid lines represent steps that are run in fragment shaders executed on the GPU whereas dashed lines represent steps that are executed on the CPU.

It can be noted from the earlier discussion that the computational complexity of the ATT algorithm is linear in the number of the pixels. Theoretically, this is the most efficient complexity that can be obtained (up to a constant factor) for a tone-mapping operation. This is because any tone-mapping algorithm needs to process each pixel in the image, and therefore, it is impossible to have a sub-linear algorithm in the number of pixels. Our GPU implementation performs most of the steps in parallel and boosts the speed by a large factor. For a typical three-channel HDR image of dimensions 512 × 768, the GPU implementation of the ATT algorithm took 0.257 second (3.9 fps) on a single core CPU whereas on an NVIDIA GeForce Titan Black GPU it took only 0.0115 second (87 fps), giving a speedup of more than 22×. The gain in speed is large for larger images. For images of size 2048 × 1536, CPU completed the task in 11.44 seconds (0.09 fps) on average, whereas GPU took 0.0425 second (24 fps), resulting in gain of 269 times in execution speed.

V. CONCLUSION

A tone-mapping operator called the Adaptive TVI-TMO ("ATT") that can map HDR intensities to a lower displayable range was presented. The operator used TVI for construction of histogram for tone mapping and an LUT to carry out mapping operations efficiently through simple linear interpolation. GPU implementation of the ATT algorithm was presented, which can perform tone mapping of typical 512 × 768 HDR color images at a rate of around 87 images per second and of 2048 × 1536 HDR color images at 24 images per second on a common hardware, thus making it potentially suitable for real-time applications. Quality assessment of the algorithm using both quantitative metrics and user studies was also presented and discussed in detail. These evaluations showed that performance of the ATT design is better than the best of the existing operators. TMQI metric's structural similarity index, measuring the capability of a TMO to preserve structure of the original scene, was quite high for all the existing operators, thus not leaving much room for improvement for the ATT algorithm. However, improvement was quite visible in TMQI naturalness index, especially for the images where other methods showed low score. For example, the ATT algorithm scored 0.75 compared to 0.21 and 0.2 scores of Larson's and Reinhard's methods, respectively, for the CrowFootGlacier image. The ATT algorithm attained highest overall TMQI scores for 159 out of 189 test images (84%) and was assessed to be the best for eight out of nine test images (90%) used for user studies. Moreover, ATT did not get very low score for any of the test images. In case the result of the ATT algorithm is not the best, it still stands close to the winner.

ACKNOWLEDGMENT

The authors would like to thank DSR for the technical and financial support.

REFERENCES

[1] E. Reinhard, G. Ward, S. Pattanaik, and P. Debevec, High Dynamic Range Imaging*: Acquisition, Display, and Image-Based Lighting*. San Mateo, CA, USA: Morgan Kaufmann, 2005.
[2] Z. Stejic, Y. Takama, and K. Hirota, "Relevance feedback-based image retrieval interface incorporating region and feature saliency patterns as visualizable image similarity criteria," *IEEE Trans. Ind. Electron.*, vol. 50, no. 5, pp. 839–852, Oct. 2003.
[3] R. T. Harding and C. H. Wu, "A method for quantization scale factor selection in MPEG2 video sequence encoding using a bilayer fuzzy expert system," *IEEE Trans. Ind. Electron.*, vol. 45, no. 1, pp. 32–37, Feb. 1998.
[4] D. T. Võ, S. Lertrattanapanich, and Y.-T. Kim, "Low line memory visually lossless compression for color images using non-uniform quantizers," *IEEE Trans. Consum. Electron.*, vol. 57, no. 1, pp. 187–195, Feb. 2011.

[5] J. Li, Y. H. Tian, T. J. Huang, and W. Gao, "Probabilistic multi-task learning for visual saliency estimation in video," *Int. J. Comput. Vis.*, vol. 90, no. 2, pp. 150–165, Nov. 2010.
[6] L. Leroy, P. Fuchs, and G. Moreau, "Visual fatigue reduction for immersive stereoscopic displays by disparity content and focus-point adapted blur," *IEEE Trans. Ind. Electron.*, vol. 59, no. 10, pp. 3998–4004, Oct. 2012.
[7] M. I. Chacon-Murguia and S. Gonzalez-Duarte, "An adaptive neural-fuzzy approach for object detection in dynamic backgrounds for surveillance systems," *IEEE Trans. Ind. Electron.*, vol. 59, no. 8, pp. 3286–3298, Jan. 2011.
[8] J. Tumblin and H. Rushmeier, "Tone reproduction for realistic images," *IEEE Comput. Graphics Appl.*, vol. 13, no. 6, pp. 42–48, Nov. 1993.
[9] F. Durand and J. Dorsey, "Fast bilateral filtering for the display of high dynamic range images," *ACM Trans. Graphics*, vol. 21, no. 3, pp. 257–266, 2002.
[10] R. Mantiuk, K. Myszkowski, and H.-P. Seidel, "A perceptual framework for contrast processing of high dynamic range images," *ACM Trans. Appl. Perception*, vol. 3, no. 3, pp. 286–308, 2006.
[11] L. Meylan and S. Susstrunk, "High dynamic range image rendering with a retinex-based adaptive filter," *IEEE Trans. Image Process.*, vol. 15, no. 9, pp. 2820–2830, Aug. 2006.
[12] N. Banić and S. Lončarić, "Color Badger: A novel retinex-based local tone mapping operator," in *Image and Signal Processing*. Cham, Switzerland: Springer, 2014, pp. 400–408.
[13] S. Ferradans, M. Bertalmio, E. Provenzi, and V. Caselles, "An analysis of visual adaptation and contrast perception for tone mapping," *IEEE Trans. Pattern Anal. Mach. Intell.*, vol. 33, no. 10, pp. 2002–2012, Mar. 2011.
[14] R. Mantiuk, S. Daly, and L. Kerofsky, "Display adaptive tone mapping," *ACM Trans. Graphics*, vol. 27, no. 3, 2008, Art. no. 68.
[15] K. Kim, J. Bae, J. Kim, "Natural HDR image tone mapping based on retinex," *IEEE Trans. Consum. Electron.*, vol. 57, no. 4, pp. 1807–1814, Nov. 2011.
[16] J. A. Ferwerda, S. N. Pattanaik, P. Shirley, and D. P. Greenberg, "A model of visual adaptation for realistic image synthesis," in *Proc. 23rd Annual Conf. Comput. Graphics Interactive Techn.*, 1996, pp. 249–258.
[17] F. Drago, K. Myszkowski, T. Annen, and N. Chiba, "Adaptive logarithmic mapping for displaying high contrast scenes," *Comput. Graphics Forum*, vol. 22, no. 3, pp. 419–426, 2003.
[18] J. H. V. Hateren, "Encoding of high dynamic range video with a model of human cones," *ACM Trans. Graphics*, vol. 25, no. 4, pp. 1380–1399, Jan. 2006.
[19] E. Reinhard and K. Devlin, "Dynamic range reduction inspired by photoreceptor physiology," *IEEE Trans. Vis. Comput. Graphics*, vol. 11, no. 1, pp. 13–24, Jan. 2005.
[20] P. Cyriac, D. Kane, and M. Bertalmío, "Perceptual dynamic range for in-camera image processing," in *Proc. British Mach. Vision Conf.,* USA, Sep. 2015, pp. 19.1–19.11.
[21] N. Banić and S. Lončarić, "Puma: A high-quality retinex-based tone mapping operator," in *Proc. Eur. Signal Process. Conf.,* 2016, pp. 943–947.
[22] M. Čadík, M. Wimmer, L. Neumann, and A. Artusi, "Evaluation of HDR tone mapping methods using essential perceptual attributes," *Comput. Graphics*, vol. 32, no. 3, pp. 330–349, 2008
[23] X. Cerdá-Company, C. A. Párraga, and X. Otazu, "Which tone-mapping operator is the best? A comparative study of perceptual quality," in *Proc. Asian Conf. Comput. Vision*, 2016, pp. 440–449.
[24] D. Lischinski, Z. Farbman, M. Uyttendaele, and R. Szeliski, "Interactive local adjustment of tonal values," in *Proc.* ACM SIGGRAPH Papers, 2006, pp. 646–653.
[25] Z. Farbman, R. Fattal, D. Lischinski, and R. Szeliski, "Edge-preserving decompositions for multi-scale tone and detail manipulation," in *Proc. ACM SIGGRAPH Papers*, 2008, pp. 67:1–67:10.
[26] S. Rahardja, F. Farbiz, C. Manders, H. Zhiyong, J. N. S. Ling, I. R. Khan, O. E. Ping, and S. Peng, "Eye HDR: Gaze-adaptive system for displaying high-dynamic-range images," in *Proc. ACM SIGGRAPH ASIA Art Gallery Emerg. Technol.*, 2009, p. 68.
[27] T. Yamauchi, T. Mikami, O. Ouda, T. Nakaguchi, and N. Tsumura, "Improvement and evaluation of real-time tone mapping for high dynamic range images using gaze information," in *Proc. Asian Conf. Comput. Vision*, 2011, pp. 440–449.
[28] E. Francois, C. Fogg, Y. He, X. Li, A. Luthra, and A. Segall, "High dynamic range and wide color gamut video coding in HEVC: Status and potential future enhancements," *IEEE Trans. Circuits Syst. Video Technol.*, vol. 26, no. 1, pp. 63–75, 2016.
[29] E. Reinhard, M. Stark, P. Shirley, and J. Ferwerda, "Photographic tone reproduction for digital images," *ACM Trans. Graphics*, vol. 21, no. 3, pp. 267–276, Jan. 2002.
[30] M. H. Kim and J. Kautz, "Consistent tone reproduction," in *Proc. 10th IASTED Int. Conf. Comput. Graphics Imaging*, D. Thalmann, Ed. Anaheim, CA, USA: ACTA, 2008, pp. 152–159.
[31] D. Kim, K. Jung, B. Ham, Y. Kim, and K. Sohn, "Normalized tone-mapping operators for color quality improvement in 3DTV," in *Proc. IEEE Conf. Ind. Electron. Appl.*, 2014, pp. 430–435.
[32] L. Lenzen and M. Christmann, "Subjective viewer preference model for automatic HDR down conversion," *Electron. Imaging*, vol. 12, pp. 191–197, 2017.
[33] B.-K. Kim, R.-H. Park, and S. Chang, "Tone mapping with contrast preservation and lightness correction in high dynamic range imaging," *Signal, Image Video Process.*, vol. 10, no. 8, pp. 1425–1432, 2016.
[34] G. Larson, H. Rushmeier, and C. Piatko, "A visibility matching tone reproduction operator for high dynamic range scenes," *IEEE Trans. Vis. Comput. Graphics*, vol. 3, no. 4, pp. 291–306, Oct.–Dec. 1997.
[35] I. R. Khan, Z. Huang, F. Farzam, and C. Manders, "Tone reproduction via histogram adjustment under controlled contrast enhancement," in *Proc. IEEE Int. Conf. Inform., Commun. Signal Process.*, 2009.
[36] H. Yeganeh and Z. Wang, "Objective quality assessment of tone-mapped images," *IEEE Trans. Image Process.*, vol. 22, no. 2, pp. 657–667, Oct. 2012.
[37] D.-C. Kim, J.-H. Yoo, W.-H. Choe, and Y.-H. Ha, "Visibility enhancement of mobile device through luminance and chrominance compensation upon hue," *IEEE Trans. Ind. Electron.*, vol. 64, no. 4, pp. 3039–3047, Dec. 2016.
[38] M. Kundu and S. Pal, "Thresholding for edge detection using human psychovisual phenomena," *Pattern Recognit. Lett.*, vol. 4, no. 6, pp. 433–441, 1986.
[39] G. Ward, "Defining dynamic range," in *Proc. ACM SIGGRAPH 2008 Classes*, 2008, pp. 30:1–30:3.
[40] The Grayscale Standard Display Function. [Online]. Available: http://dicom.nema.org/MEDICAL/DICOM/2014c/output/chtml/part14/chapter_7.html. Accessed: Sep. 22, 2017.
[41] EMPA Media Technology. [Online]. Available: http://empamedia. ethz.ch/hdrdatabase/index.php. Accessed: Sep. 22, 2017.
[42] Funt *et al.,* "HDR Dataset." [Online]. Available: http://www.cs.sfu.ca/~colour/data/funt_hdr/. Accessed: Sep. 22, 2017.
[43] H. Z. Nafchi, A. Shahkolaei, R. F. Moghaddam, and M. Cheriet, "FSITM: A feature similarity index for tone-mapped images," *IEEE Signal Process. Lett.*, vol. 22, no. 8, pp. 1026–1029, 2015.
[44] I. Buck and T. Purcell, "A toolkit for computation on GPUs," in *GPU Gems: Programming Techniques, Tips and Tricks for Real-Time Graphics*, R. Fernando, Ed. New York, NY, USA: Pearson, 2004, ch. 37.
[45] T. Scheuermann and J. Hensley, "Efficient histogram generation using scattering on GPUs," in *Proc. ACM Symp. Interactive 3D Graphics Games*, ACM New York, NY, USA, 2007.
[46] J. Hensley, T. Scheuermann, G. Coombe, M. Singh, and A. Lastra, "Fast summed-area table generation and its applications," in *Proc. Comput. Graphics Forum (Proc. Eurographics)*, Sep. 2005, vol. 24, no. 3, pp. 547–555.

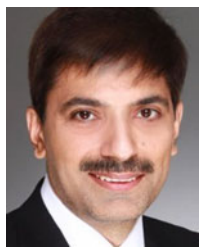

Ishtiaq Rasool Khan received the B.Sc. degree in electrical engineering from the University of Engineering and Technology, Taxila, Pakistan, in 1992, the M.S. degree in systems engineering from Quaid-i-Azam University, Islamabad, Pakistan, in 1994, and the M.S. degree in information engineering and Ph.D. degree in digital signal processing from Hokkaido University, Hokkaido, Japan, in 1998 and 2000, respectively.

He was with the University of Kitakyushu, Japan, Kyushu Institute of Technology, Japan, and Institute for Infocomm Research, A∗STAR, Singapore. He is currently a Professor with the Faculty of Computing and Information Technology, King Abdulaziz University, Jeddah, Saudi Arabia, and the University of Jeddah, Jeddah. His current research interests include high-dynamic-range imaging, data analytics, and digital filtering.

Dr. Khan was a JSPS Fellow during 2000–2002 at Hokkaido University, Japan.

Susanto Rahardja (F'11) received the B.Eng. degree from National University of Singapore, Singapore, Singapore, in 1991, and the M.Eng. and Ph.D. degrees from Nanyang Technological University, Singapore, in 1993 and 1997, respectively, all in electronic engineering.

He is currently a Chair Professor with the Northwestern Polytechnical University (NPU), Xi'an, China, under the Thousand Talent Plan of People's Republic of China. His current research interests include multimedia, signal processing, wireless communications, discrete transforms, and signal processing algorithms, implementation and optimization.

Dr Rahardja was the recipient of numerous awards, including the IEE Hartree Premium Award, the Tan Kah Kee Young Inventors' Open Category Gold award, the Singapore National Technology Award, A∗STAR Most Inspiring Mentor Award, the Finalist of the 2010 World Technology and Summit Award, the Nokia Foundation Visiting Professor Award, and the ACM Recognition of Service Award.

Muhammad Murtaza Khan received B.S. degree in electrical engineering from University of Engineering and Technology, Taxila, Pakistan, in 2000, the M.S. degree in computer software engineering from National University of Sciences and Technology, Rawalpindi, Pakistan, in 2005, and the M.S. and Ph.D. degrees in image processing from Grenoble Institute of Technology, Grenoble, France, in 2006 and 2009, respectively.

He is currently an Assistant Professor with the Faculty of Computing and Information Technology, University of Jeddah. His research interests include image processing, computer vision, machine learning and remote sensing.

Muhammad Mobeen Movania received the Ph.D. degree in advance computer graphics and visualization from Nanyang Technological University, Singapore.

After his graduation, he joined Institute for Infocomm Research, A∗STAR, Singapore as a research scientist. He is currently an Assistant Professor with DHA Suffa University, Karachi, Pakistan. His research interests include GPU-based volumetric rendering techniques, real-time soft body physics, real-time collision detection and response, and hierarchical geometric data structures.

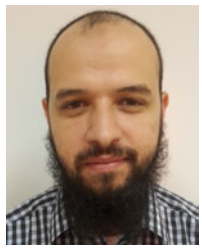

Fidaa Abed received the M.S. and Ph.D. degrees in computer science from Max-Planck-Institut für Informatik, Saarland University, Saarbrücken, Germany, in 2010 and 2014, respectively.

He was a Postdoctoral Researcher with the Mathematics Department, Technische Universität Berlin and Technische Universität Munich. He is currently an Assistant Professor with the Faculty of Computing and Information Technology, University of Jeddah, Jeddah, Saudi Arabia. His current research interests include algorithms, optimization, machine scheduling, HDR image and video encoding, and algorithmic game theory.